IEEE Access
Multidisciplinary | Rapid Review | Open Access Journal

Received 19 April 2023, accepted 29 April 2023, date of publication 8 May 2023, date of current version 16 May 2023.

Digital Object Identifier 10.1109/ACCESS.2023.3274192

METHODS

Countermeasure to Prevent Transformer Differential Protection From False Operations

PENGHUI LIU[1,2], BINGHAO JIAO[1], PENG ZHANG[3], SHAOTONG DU[1], JUN ZHU[1], AND YUNZHONG SONG[1]

[1]School of Electrical Engineering and Automation, Henan Polytechnic University, Jiaozuo 454003, China
[2]Henan Key Laboratory of Intelligent Detection and Control of Coal Mine Equipment, Jiaozuo 454003, China
[3]Key Laboratory of Smart Grid of Ministry of Education, Tianjin University, Tianjin 300072, China

Corresponding author: Penghui Liu (penghuiliu@foxmail.com)

This work was supported in part by the Fundamental Research Funds for the Universities of Henan Province under Grant NSFRF220425, in part by the Key Scientific Research Project of Henan Education Department under Grant 22B470006, in part by the Natural Science Foundation of Henan under Grant 232300420301, and in part by the Doctoral Fund Project of Henan Polytechnic University under Grant B2020-21.

ABSTRACT The reliability of the transformer differential protection is under threat from multiple interferences, including the inrush condition, the current transformer saturation condition, and the arc fault condition. For improvement, a new method is proposed to discriminate fault conditions and other non-fault conditions. Firstly, the proposed method identifies the unidirectional inrush via unidirectional index, since only it exhibits unidirectional characteristic. Then, the remaining signals are classified by the quartering-based similarity index. The quartering-based similarity index is obtained by quartering segmented fitting to overcome the drawback of overall fitting. Simulation results indicate that the proposed method is able to effectively avoid misjudgments caused by aforementioned interferences. Actual experimental tests, field data tests, and comparison analyses demonstrate its engineering adaptability and superiority.

INDEX TERMS Curve fitting, current transformers, fault currents, fault detection, inrush current, protective relaying, power system faults, power transformers, signal classification, waveform analysis.

I. INTRODUCTION

Power transformers are important components in electric power systems [1], [2], [3]. The main protection of power transformers is the differential protection which is based on Kirchhoff's current law. However, the transformer differential protection may be incorrectly tripped by magnetizing inrush condition which belongs to a kind of non-fault condition. Therefore, it is necessary to quickly distinguish the magnetizing inrush current and the fault current, before the transformer differential protection is about to act. Once a magnetizing inrush current is recognized, the differential protection will be blocked.

Conventionally, the second harmonic principle and dead-angle principle are utilized to cope with this issue. However they have been proved to be not always effective [4], [5]. Hence, various new methods are presented in the literature. They can be grouped into six categories:

Category 1: Methods based on statistical parameters. These methods construct protection criteria according to statistical numerical distribution of sampled signals [4], [5].

Category 2: Waveform similarity methods. Unlike the fault current, the magnetizing inrush waveform does not take a sinusoidal form. Based on the waveform similarity, several methods such as probabilistic distance measures [6], Kullback-Leibler divergence [7], discrete Fréchet distance [8] and Hausdorff distance [9], [10] have been investigated.

Category 3: Electrical parameter-based methods. They includes the current change ratio (CCR) and the percentage area difference (PAD) [11], the rate of phase angle [12], positive and negative sequence components [13], and the Sub-Cycle phase angle distance [14].

Category 4: Methods based on signal transform. Benefiting from their time-frequency analysis ability, signal transform

The associate editor coordinating the review of this manuscript and approving it for publication was Gerard-Andre Capolino.

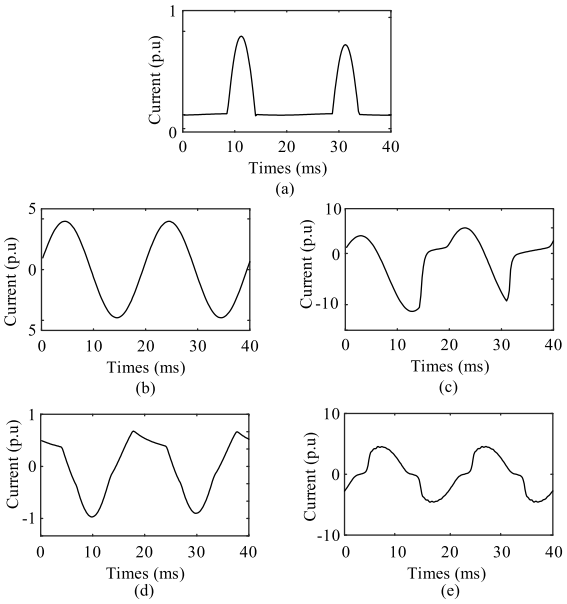

FIGURE 1. Current signal waveform of power transformers. (a) magnetizing inrush current, (b) internal fault current, (c) saturated fault current, (d) saturated inrush current, (e) arc fault current.

algorithms are widely used to discriminate inrush currents and internal fault currents [15], [16], [17], [18], [19], [20].

Category 5: Methods based on artificial intelligence algorithms, including artificial neural networks [21], [22], [23], [24], [25], fuzzy control [26], random forest [27], and K nearest neighbor-genetic [28]. Their reliability depends on the effectiveness of the used algorithms, the completeness of the training samples and the empirical knowledge.

Category 6: Other methods [29], [30], [31].

Many of them are very ingenious and interesting. However, they face challenges from one or more of following interferences.

1) Saturated fault current. If a fault current suffers current transformer (CT) saturation, its waveform on the secondary side of CT will no longer present sinusoidal features. There will be dead-angle and serious second harmonic components, as shown in Fig. 1(c). This may have adverse impacts on identification methods, such as [15], [19], [22], and [28].

2) Saturated inrush current. When affected by CT saturation, the magnetizing inrush waveform under saturation state is distorted, as shown in Fig. 1(d). The distortion changes the dead-angle feature of magnetizing inrush current, which can lead to the incorrect act of differential protections. Nonetheless, except for [17] and [26], saturated inrush current is not involved in aforementioned studies.

3) Arc fault current. An arc fault will cause nonlinear distortion, as shown in Fig. 1(e). The distorted waveform is similar to the saturated fault current. The appearance of dead-angle affects the identification of the fault current, causing the protection to be incorrectly blocked. However, this case is rarely covered in aforementioned studies.

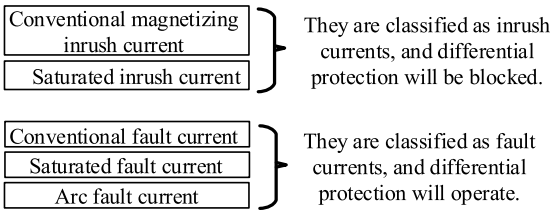

FIGURE 2. Classification of five kinds of transformer current signals.

For improvement, a new method is proposed to not only distinguish between conventional magnetizing inrush current and conventional fault current, but also address the aforementioned situations. Compared with other existing methods, the proposed method is able to more reliably work under multiple interferences, including magnetizing inrush with/without CT saturation, short-circuit faults with/without CT saturation, as well as arc faults in transformers.

II. DISTINGUISHING PRINCIPLES OF TRANSFORMER CURRENT SIGNALS

Fig. 1 displays five kinds of transformer current signals. They are taken from actual field. In this paper, they will be classified into two categories as shown in Fig. 2. Conventional fault current, saturated fault current, and arc fault current are generated by faults which must be cleared by differential protection. Conventional magnetizing inrush current and saturated inrush current are generated by non-fault condition which should not lead to the action of differential protection.

Simplified classification steps are presented as follows.

Step 1: Distinguishing unidirectional magnetizing inrush current from all other signals. After all, only the magnetizing inrush current may exhibit unidirectional waveform characteristics.

Step 2: Distinguishing bidirectional (or saturated) magnetizing inrush current from fault current of all kinds.

In short, the unidirectional magnetizing inrush signal is selected by step 1, and the rest is further classified by step 2.

The specific classification principles and procedures are presented in detail below.

A. DISTINGUISHING UNIDIRECTIONAL MAGNETIZING INRUSH CURRENT FROM ALL OTHER SIGNALS

1) PROBLEM ANALYSIS

After observing the waveform distribution pattern of these signals, it can be found that they take on two kinds of forms. One is the unidirectional current, as shown in Fig. 1(a). The other is the bidirectional current, as shown in Fig. 1(b)-(e). Hence, the signal shown in Fig. 1(a) can be easily selected by its unidirectional waveform feature. The reason for the unidirectional characteristics of the magnetizing inrush current is that part of the magnetizing inrush current contains a large amount of nonperiodic components, skewing to one side of the time axis.

It is important to note that magnetizing inrush currents are not all unidirectional. In some cases, some of them are also bidirectional, especially in Y/d connected transformers.

A unidirectional index (U_{I}) is defined to compose a quick prepositive criterion. Once it is satisfied, the differential current will be directly judged to be a magnetizing inrush current, and subsequent procedures will not be carried out.

2) UNIDIRECTIONAL INDEX

The U_{I} value is obtained by (1).

$$U_I = \left|\sum_{r=1}^{N} I_r\right| \Big/ \sum_{r=1}^{N} |I_r| \tag{1}$$

where I_r is the r-th sample value of the differential current, N is the number of samples in one fundamental frequency cycle.

The quick prepositive criterion is expressed as

$$U_I > U_{set} \tag{2}$$

The unidirectional characteristic of the waveform is expressed by the value of U_{I}. The numerator of U_{I} represents the sum of sample values within a fundamental frequency period. The denominator of U_{I} is a reference value. For the unidirectional magnetizing inrush current signal, the obtained values of the numerator and denominator in (1) are similar, so that the obtained value of U_{I} is very close to 1. Different from this, the denominator of other bidirectional current is much greater than its numerator. Consequently, the threshold U_{set} is set to 0.8. If the obtained value of U_{I} is greater than the threshold, it will be identified as a unidirectional magnetizing inrush current. Otherwise, it will go to Step 2 for the next identification.

For the convenience of following descriptions, the above identification based on the unidirectional index is referred to as the criterion 1.

B. DISTINGUISHING BIDIRECTIONAL (OR SATURATED) MAGNETIZING INRUSH CURRENT FROM FAULT CURRENT OF ALL KINDS

1) WAVEFORM FILTERING

a: FILTERING PRINCIPLE

The sinusoidal characteristic is one of the characteristics that is often used to distinguish internal fault currents from magnetizing inrush currents. It describes the difference between the differential current waveform and the standard sinusoidal waveform. As shown in Fig. 1, the waveform of fault current signals (e.g. Fig. 1(b)) approximates a sinusoidal waveform, while the waveform of magnetizing inrush current is different from the sinusoidal waveform (e.g. Fig. 1(a)).

However, the saturated fault current is an exception, due to the distortion caused by saturation. This is described in Fig. 3. The saturated fault current waveform and standard sinusoidal waveform are represented by the black scatter and red curve respectively. It is obvious that there is a difference between them, which must be considered. As shown in Fig. 3,

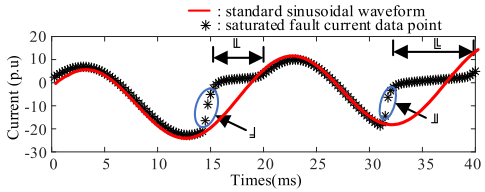

FIGURE 3. Saturated fault current waveform and standard sinusoidal waveform.

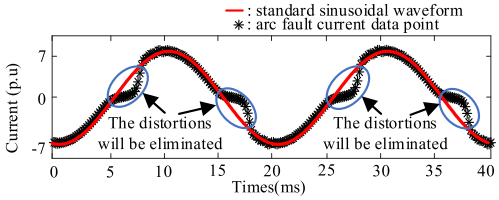

FIGURE 4. Arc fault current waveform and standard sinusoidal waveform.

these differences are mainly manifested in dead-angles produced by the distortion (e.g. ① and ②), as well as transition processes before dead-angles (e.g. ③ and ④). The reason is that the CT remanence and the nonperiodic component of the CT primary current cause CT saturation and distortion of the CT secondary current waveform. When the transformer is running with a fault, the CT saturation becomes more serious under the influence of CT remanence, which is more likely to lead to incorrect action of protection. Similarly, excessive differential current amplitude is also a cause of saturation. The above distortions easily lead to a saturated fault current being misjudged as a magnetizing inrush current, which challenges the validity of the algorithms based on sinusoidal similarity.

To solve these problems, a waveform filtering scheme is adopted to address these waveform distortions, as follows:

Firstly, eliminate data of dead-angles, such as ① and ② in Fig. 3. Then, eliminate data of transition processes near dead angles, such as ③ and ④ in Fig. 3.

After eliminating these waveform data, the difference between residual saturated fault current data and standard sinusoidal data becomes very small.

Similarly, the waveform of the arc fault current signal also deviates from the standard sinusoidal waveform. As shown in Fig. 4, the distortion type of the arc fault current is similar to the saturated fault current described above. After the waveform distortion interference is eliminated by the above two steps, the difference between residual arc fault current data and standard sinusoidal data will be greatly reduced.

b: SPECIFIC IMPLEMENTATION PROCESSES OF THE WAVEFORM FILTERING SCHEME

The maximum value M_C is obtained according to (3)

$$M_C = \max_{1 \le r \le N} (|I_r|) \tag{3}$$

where I_r is the r-th sample datum in a fundamental frequency period.

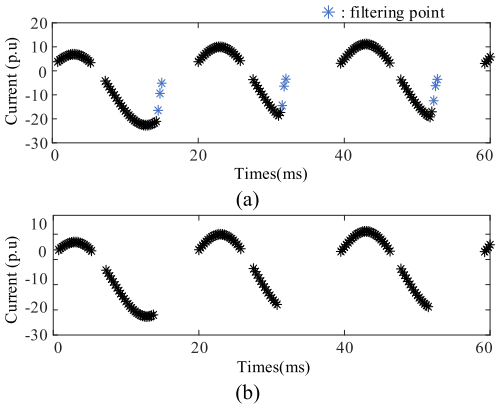

FIGURE 5. Data point of saturated fault current after interference filtering. (a) data point after eliminating dead-angles, (b) data point after eliminating transition processes near dead-angles.

The sampled data are monitored in real time. Once (4) is satisfied, the interference data will be found and filtered out. After filtering out this interference, the result of the saturated fault current is shown in Fig. 5(a).

$$|I_r| < 0.15M_C(1 \le r \le N) \tag{4}$$

It can be found that the remaining sample data after implementing this filtering step are no longer continuous. For all I_r which satisfies (4), the values of r are recorded in $\{d_h\}$ in turn.

Then, if (5) is further satisfied, $N/20$ data of transition processes near dead angles will be further eliminated.

$$(d_{\mathrm{h}} - d_{h-1}) > \frac{N}{10}\,(h = L, L-1, \cdots, 2) \tag{5}$$

where L represents the total number of remaining signal data after aforementioned data elimination is implemented.

The question is whether the transition data are on the left or the right. This paper answers this question according to the slope magnitude. If (6) is satisfied, the data on the left side will be filtered out. Otherwise, the right side is filtered out.

$$\left|I_{d_h} - I_{d_{h-\frac{N}{20}}}\right| > \left|I_{d_{h+1}} - I_{d_{h+1+\frac{N}{20}}}\right| \tag{6}$$

where h represents the value which satisfies (5).

After implementing the above waveform filtering steps, Fig. 5(b) is obtained.

2) QUARTERING-BASED SIMILARITY INDEX

The above-mentioned waveform filtering principle already deals well with the waveform distortions of the saturated fault current and the arc fault current. In this part, the interference of the saturated inrush current will be further considered. Fig. 6 shows a saturated inrush current signal after waveform filtering. A standard sinusoidal waveform is also shown as a reference. After observing these two curves, it can be found that there is no remarkable difference between the saturated inrush waveform and the standard sinusoidal waveform, which is not conducive to judgement.

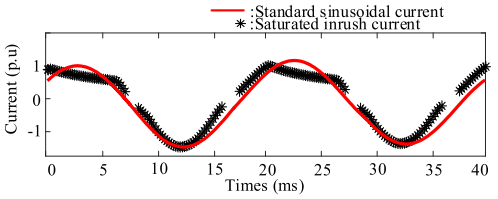

FIGURE 6. Overall fitting of a saturated inrush current signal.

To overcome these shortcomings, a quartering-based fitting scheme is proposed to take the place of overall fitting. The residual sample data after filtering are recorded in, and divided into four equal parts. They are respectively expressed as $\{I_1^*, I_2^*, \cdots, I_B^*\}$, $\{I_{B+1}^*, \cdots, I_{2B}^*\}$, $\{I_{2B+1}^*, \cdots, I_{3B}^*\}$, and $\{I_{3B+1}^*, \cdots, I_m^*\}$. The first part and the fourth part are combined to build the matrix $\boldsymbol{Y}$, and the second part and the third part are combined to build the matrix $\boldsymbol{Z}$ as (7).

$$\begin{cases} Y = [I_1^*, \cdots, I_B^*, I_{3B+1}^*, \cdots, I_m^*]^T \\ Z = [I_{B+1}^*, \cdots, I_{2B}^*, I_{2B+1}^*, \cdots, I_{3B}^*]^T \end{cases} \tag{7}$$

where the variable B can be obtained by (8).

$$B = \lfloor m/4 \rfloor \tag{8}$$

where m indicates the total number of residual sample data after implementing the above waveform filtering scheme in one cycle; the rounding symbol ($\lfloor\rfloor$) means that fractions are rounded down.

The $\boldsymbol{Y}$ and $\boldsymbol{Z}$ are fitted respectively. The $\boldsymbol{E}$ and $\boldsymbol{F}$ are obtained through the least square method as

$$\boldsymbol{E} = (\boldsymbol{Q}^T\boldsymbol{Q})^{-1}\boldsymbol{Q}^T\boldsymbol{Y} \text{ and } \boldsymbol{F} = (\boldsymbol{U}^T\boldsymbol{U})^{-1}\boldsymbol{U}^T\boldsymbol{Z} \tag{9}$$

where

$$\boldsymbol{Q} = \begin{bmatrix} 1 & \sin\frac{2\pi\times 1}{N} & \cos\frac{2\pi\times 1}{N} \\ \vdots & \vdots & \vdots \\ 1 & \sin\frac{2\pi\times B}{N} & \cos\frac{2\pi\times B}{N} \\ 1 & \sin\frac{2\pi\times(3B+1)}{N} & \cos\frac{2\pi\times(3B+1)}{N} \\ \vdots & \vdots & \vdots \\ 1 & \sin\frac{2\pi\times m}{N} & \cos\frac{2\pi\times m}{N} \end{bmatrix},$$

$$\boldsymbol{U} = \begin{bmatrix} 1 & \sin\frac{2\pi\times(B+1)}{N} & \cos\frac{2\pi\times 1}{N} \\ \vdots & \vdots & \vdots \\ 1 & \sin\frac{2\pi\times 2B}{N} & \cos\frac{2\pi\times 2B}{N} \\ 1 & \sin\frac{2\pi\times(2B+1)}{N} & \cos\frac{2\pi\times(2B+1)}{N} \\ \vdots & \vdots & \vdots \\ 1 & \sin\frac{2\pi\times 3B}{N} & \cos\frac{2\pi\times 3B}{N} \end{bmatrix}$$

$X'(k)$ and $X''(k)$ are obtained fitting results by (10).

$$\boldsymbol{V} = \boldsymbol{OE} \quad \text{and} \quad \boldsymbol{W} = \boldsymbol{OF} \tag{10}$$

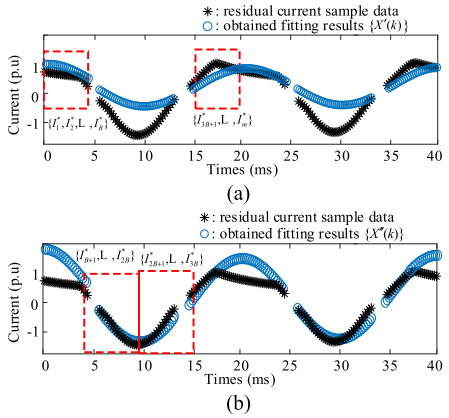

FIGURE 7. Waveform of saturated inrush currents and its fitting results. (a) fitting result of matrix Y, (b) fitting result of matrix Z.

where

$$\boldsymbol{V} = \begin{bmatrix} X'(1) \\ X'(2) \\ \vdots \\ X'(m) \end{bmatrix}, \quad \boldsymbol{W} = \begin{bmatrix} X''(1) \\ X''(2) \\ \vdots \\ X''(m) \end{bmatrix},$$

$$\boldsymbol{O} = \begin{bmatrix} 1 & \sin\dfrac{2\pi \times 1}{N} & \cos\dfrac{2\pi \times 1}{N} \\ \vdots & \vdots & \vdots \\ 1 & \sin\dfrac{2\pi \times m}{N} & \cos\dfrac{2\pi \times m}{N} \end{bmatrix}$$

According to the difference between residual current sample data and obtained fitting results, the quartering-based similarity index (Q_{SI}) is defined as

$$Q_{SI} = \frac{\left(\sqrt{\sum_{k=1}^{m}[I_k^* - X'(k)]^2} + \sqrt{\sum_{k=1}^{m}[I_k^* - X''(k)]^2}\right)}{2\sqrt{\sum_{k=1}^{m}(I_k^*)^2}} \quad (11)$$

Fig. 7 illustrates the difference between residual current sample data (I_1^* to I_m^*) and obtained fitting results. Fig. 7(a) and Fig. 7(b) respectively show the fitting results through $\boldsymbol{Y}$ and $\boldsymbol{Z}$, respectively. The difference between residual sample data and obtained fitting results is obvious. Compared with Fig. 6, the difference in Fig. 7 is more evident, which is convenient for conducting the identification.

In addition, the saturated fault currents and arc fault currents after filtering have good sinusoidal characteristics, and the obtained Q_{SI} values are always small after the above fitting is performed.

Given the above, the value of the Q_{SI} is utilized for the identification in this paper.

According to the Q_{SI}, we can distinguish magnetizing inrush current and various fault current. Concretely, if the calculated Q_{SI} of a signal is greater than the threshold (R_{set}), the signal will be identified as a magnetizing inrush current, and the differential protection will block. Otherwise, it is identified as a fault current, and the differential protection will be allowed to operate.

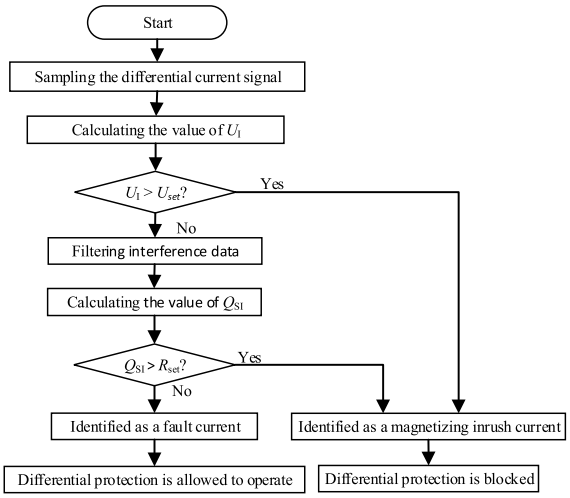

FIGURE 8. Flowchart of the proposed method.

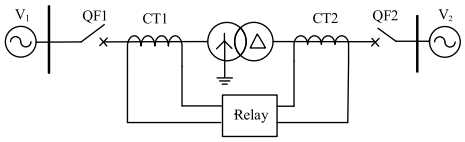

FIGURE 9. Simulation system for studies and evaluations.

It is common knowledge that a good fitting result is the same as the original signal. Therefore, the calculated Q_{SI} value in the case of an internal fault is very small, close to 0. In contrast, the calculated Q_{SI} value under magnetizing inrush current is much greater than that under fault condition. The threshold (R_{set}) aims at a certain margin, and it is determined according to sufficient simulation tests. Overall, the threshold (R_{set}) is 0.25.

For the convenience of the following descriptions, the above identification based on the quartering-based similarity index is referred to as criterion 2.

C. DISTINGUISHING PROCEDURES

According to the proposed principles and criteria, distinguishing steps are given in the following figure.

III. SIMULATION STUDIES AND EVALUATIONS

To evaluate the performance of the proposed method under various conditions, a simulation system using PSCAD/EMTDC is established as shown in Fig. 9. The simulation system includes a 220/110 kV, 100 MVA, Y/△ connected transformer. The parameter settings of the transformer and current transformer in the simulation system are shown in Table 1 and Table 2, respectively.

After operating the simulation system, secondary current signals of CTs are sampled at a sampling frequency of 4 kHz. The obtained sample data are downloaded to MATLAB

TABLE 1. Parameters of the used transformer.

Parameters	Values
Transformer MVA [MVA]	100 MVA
Base Operation Frequency [Hz]	50 Hz
Transformation ratio	220 kV / 110 kV
Winding Type	Ynd11
Positive Sequence Leakage Reactance [pu]	0.1
Saturation Enabled	Yes
Hysteresis	None/Basic Model
Air Core Reactance [pu]	0.2
Magnetizing Current [%]	1
Knee Voltage [pu]	1.17
Remanent Flux[pu]	1.2
Loop Width [%]	10

TABLE 2. Parameters of used current transformers.

Parameters	Values
Primary Turns/Secondary Turns	1/300
Secondary Resistance [Ω]	0.5
Secondary Inductance [H]	0.8e-3
Area [m^2]	2.457e-3
Path Length [m]	0.7854
Remnant Flux Density [T]	1
Burden Resistance [Ω]	0.5
Burden Inductance [H]	0.8e-6

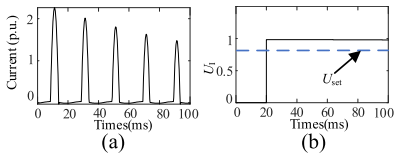

FIGURE 10. Simulation result of unidirectional magnetizing inrush current. (a) current signal, (b) obtained unidirectional index.

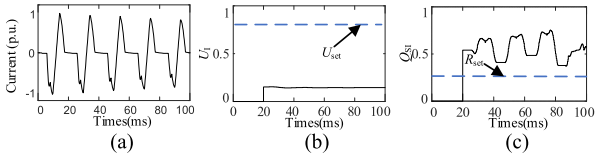

FIGURE 11. Simulation result of bidirectional magnetizing inrush current. (a) current signal, (b) obtained unidirectional index, (c) obtained quartering-based similarity index.

software where the proposed method is implemented. For different kinds of signals, the test results are as follows.

A. CONVENTIONAL MAGNETIZING INRUSH CURRENT

Magnetizing inrush currents are generated due to the remanent magnetism of the power transformer and the no-load closing time. The closing angle can affect the waveform characteristics of the inrush current, while the remanent magnetism mainly affects its amplitude. According to the simulation model, two different forms of inrush currents are obtained and shown in Fig. 10 and Fig. 11.

According to the proposed discrimination steps, the U_{I} values of the current signal data, as shown in Fig. 10(a), are calculated, and the results are shown in Fig. 10(b). The dotted blue line indicates the threshold U_{set}. It is easy to find that the

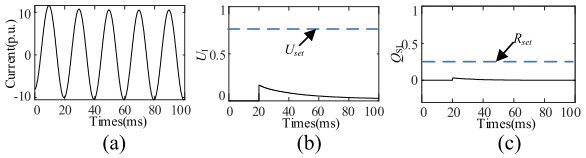

FIGURE 12. Simulation result of the internal fault current. (a) current signal, (b) obtained unidirectional index, (c) obtained quartering-based similarity index.

obtained U_{I} values are always higher than the threshold U_{set}. According to the previously proposed criterion 1, the signal will be judged as a unidirectional magnetizing inrush current.

For the bidirectional magnetizing inrush current signal in Fig. 11(a), the calculated U_{I} values are always less than the threshold U_{set}, as shown in Fig. 11(b), which confirms that the signal is identified as a bidirectional signal. Then, a further judgment is conducted according to the previously proposed criterion 2. As shown in Fig. 11(c), the obtained Q_{SI} values are always greater than the threshold R_{set}. Therefore, the signal will be further identified as a bidirectional magnetizing inrush current.

Additionally, different iron saturation curves of the iron core can be obtained by varying the air core reactance, knee voltage. In this section, various magnetizing inrush conditions with different iron saturation curves, magnetizing currents and remanent fluxes are simulated to test the correctness of the proposed detection method. The test results indicate that the method in this paper is able to accurately identify various conventional inrush currents and block the transformer differential protection.

B. INTERNAL THREE-PHASE SHORT-CIRCUIT FAULT CURRENT

Through the simulation model, a three-phase short-circuit fault located in the differential protection zone is simulated, and the obtained differential current signal is shown in Fig. 12(a). Here, phase A is used as an example to test the proposed method.

According to the sample data of this current signal, calculated U_{I} values are presented in Fig. 12(b) in graphic form. These obtained values of U_{I} are always in the region less than U_{set}. On the basis of the proposed distinguishing procedures, this signal needs to be further classified by means of the Q_{SI} mentioned in criterion 2. The calculated results of the Q_{SI} are shown in Fig. 12(c). It is clear that the threshold R_{set} is larger than the obtained values of Q_{SI}, so that the signal will be classified as a fault current. There is a large margin between them, which can avoid misjudgment.

C. MAGNETIZING INRUSH CURRENT WITH CT SATURATION

After the transformer produces a magnetizing inrush current, CT is susceptible to the influence of the aperiodic component of the magnetizing inrush current and CT remanence, resulting in the saturation phenomenon and distortion of

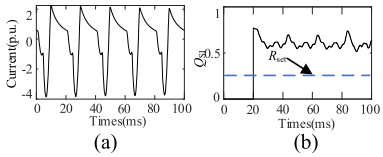

FIGURE 13. Simulation result of magnetizing inrush current with CT saturation. (a) current signal, (b) obtained quartering-based similarity index.

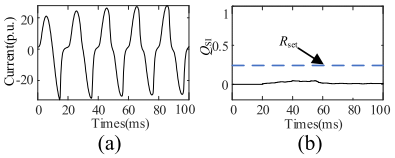

FIGURE 14. Simulation result of internal fault current with CT saturation. (a) current signal, (b) obtained quartering-based similarity index.

the secondary current of CT. This has an adverse effect on transformer protection. However, the existing studies are less involved in the CT saturation interference situation, and the existing methods are weak against CT saturation interference.

In this section, the current transformer ratio of 300 A / 5 A is selected to simulate the CT saturation case through PSCAD software. The simulation experiment of no-load closing with fault is carried out on the high-voltage side of the transformer. The saturated inrush wave obtained on the secondary side of the CT is shown in Fig. 13. Waveform distortion can be obviously observed in the figure, and there is no dead-angle. According to the unidirectional index in criterion 1, the current signal is determined to be a bidirectional current. Then, based on criterion 2, the Q_{SI} values are calculated and shown in Fig. 13(b). Given that the calculated Q_{SI} values are greater than R_{set}, the signal will be judged to be a magnetizing inrush current.

Similarly, different saturation excitation inrush currents can be obtained by varying the number of turns on the primary and secondary sides of the CT, the area and the burden resistance in Table 2. The method proposed in this study successfully determined them as inrush currents and blocked the transformer differential protection.

D. INTERNAL FAULT CURRENT WITH CT SATURATION

To simulate the short-circuit fault with CT saturation, the ratio of CT is set as 600 A / 5 A. After implementing the simulation, the saturated fault current signal shown in Fig. 14(a) is obtained. The waveform of this signal is no longer strictly sinusoidal, and there are dead-angles near zero crossing points.

The signal is judged as a bidirectional current by criterion 1. Then, the Q_{SI} values are calculated by criterion 2. According to the calculated Q_{SI} values, it is determined that the current signal is a fault current.

Various saturated fault currents are simulated by varying the parameters in Table 2. The proposed method successfully determines them as fault currents.

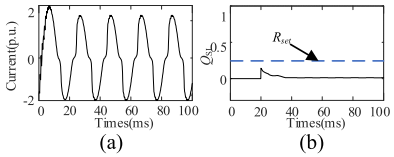

FIGURE 15. Simulation result of arc fault current. (a) current signal, (b) obtained quartering-based similarity index.

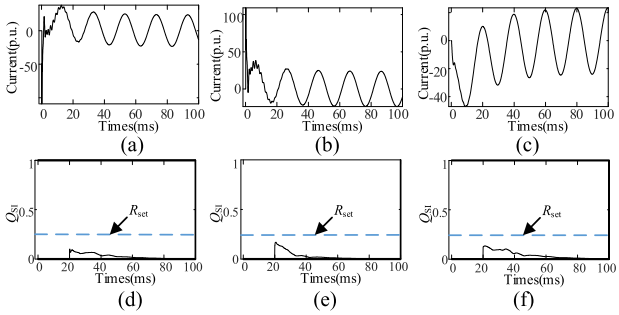

FIGURE 16. Transformer internal short-circuit fault simulation results with the presence of converter-interfaced sources. (a) obtained current 1, (b) obtained current 2, (c) obtained current 3, (d) Q_{SI} value for current 1, (e) Q_{SI} value for current 2, (f) Q_{SI} value for current 3.

E. ARC FAULT CURRENT

In this paper, the Mayr model is selected to simulate arc fault. After all, it is considered to be a common and practical arc model. In the Mayr model, the arc time constant is 0.6 ms, the heat dissipation power is 3.8 MW, the arc conductivity is 1000 S, and the grounding resistance is 100 Ω. The arc model based on Mayr theory is connected to a side of the transformer. After no-load closing the transformer with an arc fault, the arc fault current is generated. The obtained current signal and calculated values Q_{SI} are shown in Fig. 15. Due to $Q_{SI} < R_{set}$, the signal is recognized as a fault current by the proposed method. This is consistent with the default case.

F. OTHER INTERFERENCE TEST

In order to further verify the effectiveness of the algorithm, transformer internal short-circuit fault simulation tests with the presence of converter-interfaced sources are carried out. Obtained transformer differential current signals are shown in Fig. 16(a)-(c), and changing values of computed Q_{SI} are displayed in Fig. 16(d)-(f). Calculated Q_{SI} values are always less than R_{set}, so these signals will be accurately judged as fault currents.

What needs illustration is that this paper mainly focuses on magnetizing inrush with/without CT saturation, short-circuit fault with/without CT saturation, as well as arc fault in transformers. For other interference cases, further research is still needed in the follow-up work.

IV. EXPERIMENT TEST STUDIES

Three experimental ways are used to evaluate the immunity from interference and the reliability in practical engineering.

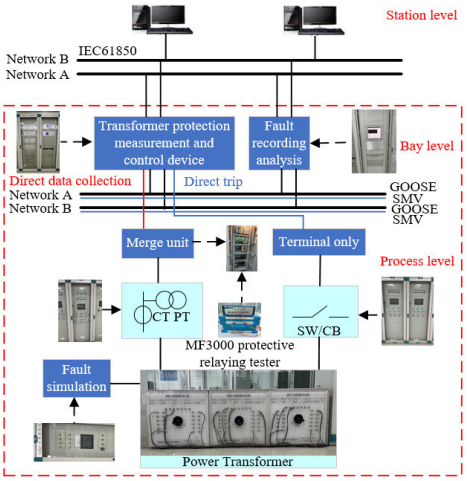

FIGURE 17. Connection diagram of actual transformer test.

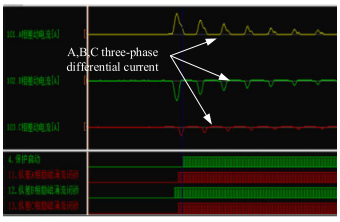

FIGURE 18. Recording analysis diagram.

A. EXPERIMENT WAY 1: ACTUAL TRANSFORMER TEST

An actual transformer simulation test is carried out in the Power System Dynamic Simulation Laboratory of a Chinese university. The experimental logical diagram for obtaining magnetizing inrush current signals and internal fault current signals is shown in Fig. 17. Three single-phase three-winding 6.67 kVA 50 Hz transformers are used to compose a 1000 V/1000 V/400 V Y/Y/△ three-phase transformer.

Specifically, a magnetizing inrush current is generated through no-load closing the transformer, while a two-phase short-circuit fault is set to generate a fault current through the fault simulation cabinet located on the high voltage side of the transformer. It should be noted that the existing transformer protection device uses the second harmonic restraint principle to identify signals. After this experiment, the existing transformer protection device displays event reports, and the wave recorder uploads the signal waveform. The obtained information is shown in Fig. 18 and Fig. 19, which indicates the ability of the existing device to identify the conventional magnetizing inrush current and fault current. The proposed method is also used to address these current signals, and the correct test results are also obtained.

B. EXPERIMENT WAY 2: ACTUAL DATA PLAYBACK TEST

During previous study works, several field recorded signal data (COMTRADE file) were obtained from a higher voltage level system in the actual field. In this experimental way, these actual field data are sent again back to the protective devices by means of a MP3000 protective relaying tester.

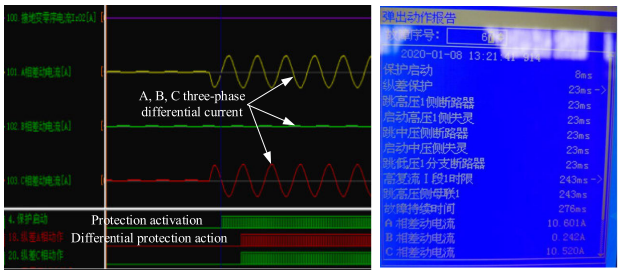

FIGURE 19. Test result of internal fault current.

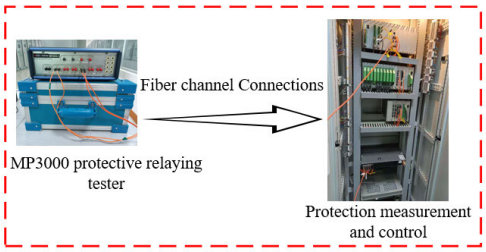

FIGURE 20. Fiber channel connection diagram of the signal playback experiment.

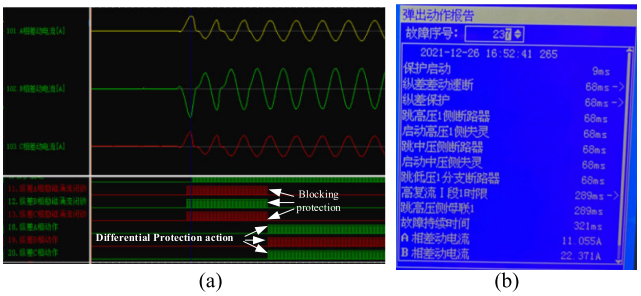

FIGURE 21. Test result of the fault with CT saturation.

The transient playback function of the protective relaying tester is used to playback the actual field recorded signal data (from a 220 kV/69 kV/10.5 kV, 120 MVA transformer) to evaluate the influence of CT saturation interference. The connection diagram is shown in Fig. 20. Due to CT saturation interference, the protection action time is delayed by 45 ms, so that the fault cannot be removed in time by the existing transformer protection device.

The same actual field recorded signals are used to test the proposed method, and correct results similar to those in Fig. 14 are obtained. Compared with Fig. 21, the proposed method operates quickly without delay. Besides, other field recorded signals from transformers of other voltage levels and capacities (e.g. 535 kV/210.4 kV, 892.8 MVA; 110 kV/10.5 kV, 20 MVA) are also used to test the proposed method, the obtained Q_{SI} values proved the practicability of the proposed method in practical engineering. Due to space limitation, they have not listed here.

C. EXPERIMENT WAY 3: FAULT TEST BY USING AN EXPERIMENTAL PLATFORM

The arc fault experimental platform as shown in Fig. 22(a) is set up. The experimental platform is mainly composed

TABLE 3. Test results for different signals and comparisons.

Classification	Second harmonic restraint		Dead-angle principle		Waveform similarity		The proposed method		
	Harmonic ratio (threshold value: 15%)	Result	Dead-angle size (threshold value: 65°)	Result	R^2 (threshold value: 0.85)	Result	U_I (U_{set} =0.80)	Q_{SI} (R_{set} =0.25)	Result
Inrush current (unidirectional)	58%	Right	135°	Right	0.4763	Right	0.98		Right
Inrush current (bidirectional)	56%	Right	130°	Right	0.4223	Right	0.15	0.57	Right
Internal fault current	0%	Right	0°	Right	0.9998	Right	0.18	0.02	Right
Saturated inrush current	64%	Right	10°	Wrong	0.9423	Wrong	0.01	0.37	Right
Saturated fault current	51%	Wrong	90°	Wrong	0.8632	Right	0.06	0.02	Right
Arc fault current	0%	Right	96°	Wrong	0.9512	Right	0.03	0.05	Right

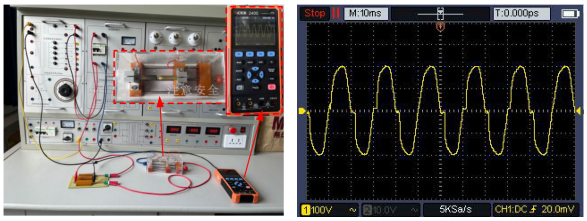

(a) (b)

FIGURE 22. Obtained arc fault current via experiment. (a) experiment platform, (b) waveform of obtained current.

of 220 V AC power supply, arc generation device, power resistor, acquisition probe and oscilloscope. One end of the arc generation device is a copper rod, and the other end is a carbon rod. After the circuit is energized, the copper rod moves slowly toward the carbon rod. When the copper rod is very close to the carbon rod, an arc fault current is produced. Then, the oscilloscope collects the arc current by measuring the sampling resistor. The obtained arc current signal is shown in Fig. 22(b), and test results for different kinds of algorithms are listed in the last row of Table 3.

V. COMPARISONS AND ANALYSES

A. PERFORMANCE COMPARISON WITH TRADITIONAL METHODS

In this section, 20 ms data of the aforementioned experiment signals after protection startup are selected and imported into MATLAB. For comparison, these data are used to assess the performance of the traditional second harmonic restraint principle, traditional dead-angle principle and the method proposed in this paper. The results are listed in Table 3.

Existing methods have disadvantages in the face of CT saturation and arc fault interference. The second harmonic restraint principle fails to correctly identify the saturated fault current, which also leads to the failure shown in Fig. 21. The dead-angle principle also misjudges the saturated inrush current, saturated fault current, and arc fault current. However, the proposed method does not have these problems.

B. PERFORMANCE COMPARISON WITH METHODS BASED ON THE WAVEFORM SIMILARITY PRINCIPLE

In recent years, methods based on the waveform similarity principle have been proposed to improve the action accuracy of transformer differential protection. Commonly, these algorithms fit all current signal data in a cycle as a whole, and then the coefficient of sinusoidal similarity (R^2) is calculated.

The aforementioned simulation and experimental signals are also fitted and analyzed. The coefficient of sinusoidal similarity is used as the basis of judgment. Results are obtained as shown in Table 3. It can be found that the methods based on the waveform similarity principle will misjudge the saturated inrush current as a fault current.

In contrast, there is no misjudgment caused by the method proposed in this paper, as shown in Table 3.

VI. CONCLUSION

This paper presented a novel discrimination method based on a unidirectional index and quartering-based similarity index. It can be applied in intelligent substation as a countermeasure to prevent transformer differential protections from false operations caused by multiple interferences, including magnetizing inrush conditions, CT saturation conditions, and arc fault conditions.

Concretely, the unidirectional index can effectively detect and identify unidirectional inrush signals. The waveform difference between saturated inrush current and the standard sinusoidal current is not significant, which may cause the overall fitting fit to produce incorrect results. The quartering-based fitting and the Q_{SI} value can overcome this shortcoming. The Q_{SI} value of bidirectional inrush current or saturated inrush current is significantly greater than that of internal fault current, saturated fault current, or arc fault current. Therefore, the quartering-based similarity index can be utilized to implement further classification.

The method based on waveform similarity principle, as well as traditional methods including the second harmonic restraint principle and dead-angle principle, may face misjudgments, due to one or more of the aforementioned interferences, which lead to the false operation or delay operation of transformer differential protections. Whereas, the proposed method has been proved to be more advantageous in dealing with these interferences.

This paper mainly focuses on aforementioned interferences. For other interference cases, further research is still needed in the follow-up work.

REFERENCES

[1] I. Žiger, B. Trkulja, and Ž. Štih, "Determination of core losses in open-core power voltage transformers," *IEEE Access*, vol. 6, pp. 29426–29435, 2018, doi: 10.1109/ACCESS.2018.2838446.

[2] J. Liu, H. Zeng, W. Niu, P. Chen, K. Xu, P. Zeng, L. Zhao, and S. Lin, "State identification of transformer under DC bias based on wavelet singular entropy," *IEEE Access*, vol. 9, pp. 58944–58952, 2021, doi: 10.1109/ACCESS.2021.3072913.

[3] S. E. Zirka, D. Albert, Y. I. Moroz, and H. Renner, "Further improvements in topological transformer model covering core saturation," *IEEE Access*, vol. 10, pp. 64018–64027, 2022, doi: 10.1109/ACCESS.2022.3183279.

[4] L. L. Zhang, Q. H. Wu, T. Y. Ji, and A. Q. Zhang, "Identification of inrush currents in power transformers based on higher-order statistics," *Electr. Power Syst. Res.*, vol. 146, pp. 161–169, May 2017, doi: 10.1016/j.epsr.2017.01.029.

[5] C. Mo, T. Y. Ji, L. L. Zhang, and Q. H. Wu, "Equivalent statistics based inrush identification method for differential protection of power transformer," *Electr. Power Syst. Res.*, vol. 203, Feb. 2022, Art. no. 107664, doi: 10.1016/j.epsr.2021.107664.

[6] M. Tajdinian and H. Samet, "Application of probabilistic distance measures for inrush and internal fault currents discrimination in power transformer differential protection," *Electr. Power Syst. Res.*, vol. 193, Apr. 2021, Art. no. 107012, doi: 10.1016/j.epsr.2020.107012.

[7] M. Tajdinian and H. Samet, "Divergence distance based index for discriminating inrush and internal fault currents in power transformers," *IEEE Trans. Ind. Electron.*, vol. 69, no. 5, pp. 5287–5294, May 2022, doi: 10.1109/TIE.2021.3082071.

[8] H. Weng, S. Wang, Y. Wan, X. Lin, Z. Li, and J. Huang, "Discrete Fréchet distance algorithm based criterion of transformer differential protection with the immunity to saturation of current transformer," *Int. J. Electr. Power Energy Syst.*, vol. 115, Feb. 2020, Art. no. 105449, doi: 10.1016/j.ijepes.2019.105449.

[9] H. L. Weng, S. Wang, X. N. Lin, L. Chen, J. G. Huang, and Z. X. Li, "Waveform similarity based transformer phase differential protection against current transformer saturation," *Autom. Electr. Power Syst.*, vol. 43, no. 4, pp. 132–138, 2019.

[10] H. Weng, S. Wang, X. Lin, Z. Li, and J. Huang, "A novel criterion applicable to transformer differential protection based on waveform sinusoidal similarity identification," *Int. J. Electr. Power Energy Syst.*, vol. 105, pp. 305–314, Feb. 2019, doi: 10.1016/j.ijepes.2018.08.027.

[11] A. A. A. Etumi and F. J. Anayi, "Current signal processing-based methods to discriminate internal faults from magnetizing inrush current," *Electr. Eng.*, vol. 103, no. 1, pp. 743–751, Feb. 2021, doi: 10.1007/s00202-020-01115-2.

[12] H. Samet, M. Shadaei, and M. Tajdinian, "Statistical discrimination index founded on rate of change of phase angle for immunization of transformer differential protection against inrush current," *Int. J. Electr. Power Energy Syst.*, vol. 134, Jan. 2022, Art. no. 107381, doi: 10.1016/j.ijepes.2021.107381.

[13] A. M. Shah, B. R. Bhalja, and R. M. Patel, "New protection scheme for power transformer based on superimposed differential current," *IET Gener., Transmiss. Distrib.*, vol. 12, no. 14, pp. 3587–3595, Aug. 2018, doi: 10.1049/iet-gtd.2018.0296.

[14] M. Tajdinian, H. Samet, and Z. M. Ali, "A sub-cycle phase angle distance measure algorithm for power transformer differential protection," *Int. J. Electr. Power Energy Syst.*, vol. 137, May 2022, Art. no. 107880, doi: 10.1016/j.ijepes.2021.107880.

[15] E. Ali, O. P. Malik, S. Abdelkader, A. Helal, and H. Desouki, "Experimental results of ratios-based transformer differential protection scheme," *Int. Trans. Electr. Energy Syst.*, vol. 29, no. 11, Nov. 2019, doi: 10.1002/2050-7038.12114.

[16] A. Roy, D. Singh, R. K. Misra, and A. Singh, "Differential protection scheme for power transformers using matched wavelets," *IET Gener., Transmiss. Distrib.*, vol. 13, no. 12, pp. 2423–2437, Jun. 2019, doi: 10.1049/iet-gtd.2018.6305.

[17] S. K. Murugan, S. P. Simon, K. Sundareswaran, P. S. R. Nayak, and N. P. Padhy, "An empirical Fourier transform-based power transformer differential protection," *IEEE Trans. Power Del.*, vol. 32, no. 1, pp. 209–218, Feb. 2017, doi: 10.1109/TPWRD.2016.2575981.

[18] D. Guillen, J. Olveres, H. Esponda, B. Escalante-Ramirez, V. Torres-García, and R. Tapia-Olvera, "Hermite transform-based algorithm to discriminate magnetizing currents in transformers," *Sustain. Energy, Grids Netw.*, vol. 27, Sep. 2021, Art. no. 100493, doi: 10.1016/j.segan.2021.100493.

[19] R. P. Medeiros, F. B. Costa, K. M. Silva, J. D. J. C. Muro, J. R. L. Junior, and M. Popov, "A clarke-wavelet-based time-domain power transformer differential protection," *IEEE Trans. Power Del.*, vol. 37, no. 1, pp. 317–328, Feb. 2022, doi: 10.1109/TPWRD.2021.3059732.

[20] M. Tajdinian, H. Samet, and Z. M. Ali, "Differential protection algorithm founded on Kalman filter-based phase tracking," *IEEE Trans. Instrum. Meas.*, vol. 71, pp. 1–9, 2022, doi: 10.1109/TIM.2021.3137565.

[21] S. Afrasiabi, M. Afrasiabi, B. Parang, M. Mohammadi, H. Samet, and T. Dragicevic, "Fast GRNN-based method for distinguishing inrush currents in power transformers," *IEEE Trans. Ind. Electron.*, vol. 69, no. 8, pp. 8501–8512, Aug. 2022, doi: 10.1109/TIE.2021.3109535.

[22] H. Balaga, N. Gupta, and D. N. Vishwakarma, "GA trained parallel hidden layered ANN based differential protection of three phase power transformer," *Int. J. Electr. Power Energy Syst.*, vol. 67, pp. 286–297, May 2015, doi: 10.1016/j.ijepes.2014.11.028.

[23] Z. Li, Z. Jiao, and A. He, "Knowledge-based artificial neural network for power transformer protection," *IET Gener., Transmiss. Distrib.*, vol. 14, no. 24, pp. 5782–5791, Dec. 2020, doi: 10.1049/iet-gtd.2020.0542.

[24] S. Afrasiabi, M. Afrasiabi, B. Parang, and M. Mohammadi, "Designing a composite deep learning based differential protection scheme of power transformers," *Appl. Soft Comput.*, vol. 87, Feb. 2020, Art. no. 105975, doi: 10.1016/j.asoc.2019.105975.

[25] S. K. Murugan, S. P. Simon, and R. R. Eapen, "A novel signal localized convolution neural network for power transformer differential protection," *IEEE Trans. Power Del.*, vol. 37, no. 2, pp. 1242–1251, Apr. 2022, doi: 10.1109/TPWRD.2021.3080927.

[26] D. Bejmert, W. Rebizant, and L. Schiel, "Transformer differential protection with fuzzy logic based inrush stabilization," *Int. J. Electr. Power Energy Syst.*, vol. 63, pp. 51–63, Dec. 2014, doi: 10.1016/j.ijepes.2014.05.056.

[27] A. M. Shah and B. R. Bhalja, "Fault discrimination scheme for power transformer using random forest technique," *IET Gener., Transmiss. Distrib.*, vol. 10, no. 6, pp. 1431–1439, Apr. 2016, doi: 10.1049/iet-gtd.2015.0955.

[28] P. B. Thote, M. B. Daigavane, P. M. Daigavane, and S. P. Gawande, "An intelligent hybrid approach using KNN-GA to enhance the performance of digital protection transformer scheme," *Can. J. Electr. Comput. Eng.*, vol. 40, no. 3, pp. 151–161, Summer 2017, doi: 10.1109/CJECE.2016.2631474.

[29] R. Dashti, A. Khoshkhoo, H. R. Parish, and H. R. Shaker, "A new operational characteristic for diagnosing the healthy and faulty currents of power transformers," *Electr. Power Syst. Res.*, vol. 203, Feb. 2022, Art. no. 107649, doi: 10.1016/j.epsr.2021.107649.

[30] H. Weng, Y. Guo, Y. Liu, H. Li, Z. Li, and J. Huang, "Normalized dynamic time warping distance based auxiliary restraint scheme for restricted earth fault protection of converter transformers," *IEEE Trans. Power Del.*, vol. 37, no. 3, pp. 1476–1487, Jun. 2022, doi: 10.1109/TPWRD.2021.3089156.

[31] P. Han, Q. Tong, Y. Wang, Z. Chen, W. Yang, D. Hu, H. Wu, and J. Zhang, "An inrush current suppression strategy for UHV converter transformer based on simulation of magnetic bias," *IEEE Trans. Power Del.*, vol. 37, no. 6, pp. 5179–5189, Dec. 2022, doi: 10.1109/TPWRD.2022.3173431.

PENGHUI LIU received the B.S. degree in electrical engineering from Henan Polytechnic University, Jiaozuo, China, in 2014, and the Ph.D. degree in electrical engineering from Hunan University, Changsha, China, in 2019.

He is currently with the School of Electrical Engineering and Automation, Henan Polytechnic University, and with the Henan Key Laboratory of Intelligent Detection and Control of Coal Mine Equipment, Jiaozuo, China. His research interests include power system monitoring and protection.

BINGHAO JIAO was born in Henan, China, in 1996. He is currently pursuing the B.Sc. degree with the School of Electrical Engineering and Automation, Henan Polytechnic University, Jiaozuo, China. His research interest includes power system relay protection.

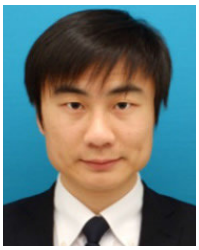

PENG ZHANG received the B.S. and M.S. degrees from Tianjin University, Tianjin, China, in 2008 and 2010, respectively, and the Ph.D. degree from Kyushu University, Fukuoka ken, Japan, in 2013.

He is currently with the Key Laboratory of Smart Grid, Tianjin University. His research interests include operation and optimization of integrated energy system.

SHAOTONG DU received the B.S. and M.S. degrees from Henan Polytechnic University, Jiaozuo, China, in 2008 and 2011, respectively, and the Ph.D. degree from the China University of Mining and Technology, Xuzhou, China, in 2015.

He is currently with the School of Electrical Engineering and Automation, Henan Polytechnic University, Jiaozuo, China. His research interests include smart grids and power equipment automation.

JUN ZHU received the B.S. and Ph.D. degrees from Inner Mongolia Agricultural University, Inner Mongolia, China, in 2005 and 2010, respectively.

He is currently an Associate Professor with the School of Electrical Engineering and Automation, Henan Polytechnic University, Jiaozuo, China. His research interests include distributed generation and intelligent equipment.

YUNZHONG SONG received the Ph.D. degree from Zhejiang University, China, in 2006. He is currently a Full Professor with the School of Electrical Engineering and Automation, Henan Polytechnic University. He has been a Visiting Professor with the Chinese Academy of Sciences (CAS) and a Visiting Scholar with Umea University, Sweden. His research interests include intelligent systems and networked systems control. He was the winner of the 2017 Best Paper Award of International Conference on Artificial Life and Robotics (ICAROB), Miyazaki, Japan.